## **Nanoscale**



PAPER View Article Online
View Journal | View Issue



Cite this: Nanoscale, 2018, 10, 4004

# Design of highly selective ethanol dehydration nanocatalysts for ethylene production†

Natalie Austin, Pavlo Kostetskyy and Giannis Mpourmpakis \*\*D\*

Rational design of catalysts for selective conversion of alcohols to olefins is key since product selectivity remains an issue due to competing etherification reactions. Using first principles calculations and chemical rules, we designed novel metal-oxide-protected metal nanoclusters ( $M_{13}X_4O_{12}$ , with M=Cu, Ag, and Au and X=Al, Ga, and In) exhibiting strong Lewis acid sites on their surface, active for the selective formation of olefins from alcohols. These symmetrical nanocatalysts, due to their curvature, show unfavorable etherification chemistries, while favoring the olefin production. Furthermore, we determined that water removal and regeneration of the nanocatalysts is more feasible compared to the equivalent strong acid sites on solid acids used for alcohol dehydration. Our results demonstrate an exceptional stability of these new nanostructures with the most energetically favorable being Cu-based. Thus, the high selectivity and stability of these in-silico-predicted novel nanoclusters (e.g.  $Cu_{13}Al_4O_{12}$ ) make them attractive catalysts for the selective dehydration of alcohols to olefins.

Received 21st November 2017, Accepted 18th January 2018 DOI: 10.1039/c7nr08678d

rsc.li/nanoscale

#### Introduction

Earth-abundance and the low cost of plant biomass make it a viable substitute to fossil fuels as carbon-neutral feedstock for the production of fuels and chemicals. Generally, its high oxygen content is an issue in the field of biomass processing, forming a range of alcohols, polyols and phenols with one or more hydroxyl (OH) functionalities. The high oxygen content of these biomass products has been shown to lower the overall value and cause processing complications. 1-4 Unit operations to reduce the oxygen content of biomass products are important for improving the overall efficiency and process economics. Catalytic upgrading of oxygenates is a vital component in biomass processing operations, characterized by cleavage of oxygenate C-O bonds. Dehydration of aliphatic alcohols via acid-based catalysis is an important, industrially relevant reaction. Solid acids, including metal oxides, zeolites, and polyoxometalates, have been shown to be active alcohol dehydration catalysts.<sup>5-9</sup> Dehydration reactions occur at moderate temperatures (~500 K) and proceed via unimolecular and bimolecular pathways, forming olefin and ether products. 9-13 The formation of acetaldehyde (via dehydrogenation reactions) should not be expected in these catalytic systems, as it has been shown in recent computational<sup>9</sup> and experimental<sup>13</sup> studies that for γ-Al<sub>2</sub>O<sub>3</sub>, which exhibits undercoordinated, Lewis

Department of Chemical Engineering, University of Pittsburgh, Pittsburgh, PA 15261, USA. E-mail: gmpourmp@pitt.edu

†Electronic supplementary information (ESI) available. See DOI: 10.1039/c7nr08678d

surface acid sites, the formation of ethers and olefins is majorly preferred over aldehydes. Ethylene and diethyl ether (DEE) are ethanol dehydration products and precursors in the production of polymers, solvents, fuels, and specialty chemicals.<sup>3,4</sup> Solid acid catalysts currently used for alcohol dehydration are generally limited in selectivity control therefore requiring the tuning of operating conditions.<sup>11,12</sup> The design of highly stable, selective and active heterogeneous catalysts is the "Holy Grail" in catalysis and in processes of industrial relevance, such as the dehydration of ethanol to ethylene (polymer building blocks).

Lewis (LA) and Brønsted (BA) acid catalysts are active in alcohol dehydration to olefins, with the preferred reaction mechanism being primarily a function of nature of active sites and substitution of the reacting alcohol. Both LA- and BA-catalyzed dehydration reactions are characterized by the formation of carbenium ion (CI) intermediates in the rate-determining steps of the reaction pathway. S,8,14 Gamma alumina  $(\gamma$ -Al<sub>2</sub>O<sub>3</sub>) is a heterogeneous LA catalyst that has been shown to be one of the strongest among acidic oxides. The coordination environment of alumina surface sites plays a key role in the catalyst reactivity. A recent computational study has shown the tricoordinated aluminum sites (Al<sup>CN3</sup>) to be most acidic 15,16 and has been shown to exist on the (110) surface terminations of  $\gamma$ -Al<sub>2</sub>O<sub>3</sub>. T-19

The two reaction pathways for alcohol dehydration (DEE vs. ethylene) compete in selectivity at moderate reaction temperatures. The selectivity towards the ether pathway increases at lower temperatures and higher reactant pressures. In addition, selectivity has also been shown to be a

Nanoscale

function of alcohol chain length and substitution, preferring olefin formation with more substituted species - i.e. more

stable carbenium ion intermediates. Specifically, Kang et al. 12 reported a ~90% olefin selectivity increase from ethanol to isobutanol under identical reaction conditions, indicating that the molecular structure of reactants as well as surface sites strongly affect the observed rates. Along with this complexity, we pose a question: can we design active and selective catalysts that exhibit high olefin selectivity? Specifically, the goal is to design a catalyst capable of preferentially catalyzing the ethylene route. To the best of our knowledge, this work is the first to show rational design of mixed metal-oxide-protected metal nanocluster catalysts with structure-based selectivity towards the olefin pathway. Specifically, we demonstrate that one can take advantage of the high curvature of nanoparticles, stabilized by metal oxide complexes with generated acid sites apart from each other that do not favor bimolecular reactions, responsible for ether production.

### Computational methods

Alcohol dehydration towards olefin and ether formation was investigated on tri-coordinated Lewis acid sites of metal oxides  $XO_3$ , (X = Al, Ga, and In), stabilized on  $M_{13}$  icosahedral (initially) clusters (M = Ag, Au, and Cu). The structure of the optimized M<sub>13</sub>X<sub>4</sub>O<sub>12</sub> nanoclusters is shown in Fig. 1. Systems composed of metal oxides supported on transition metals have been successfully used to investigate the industrially relevant reactions such as CO oxidation and the water gas shift reaction (WGS).<sup>20-23</sup> We investigated the structural, electronic and catalytic properties of these nanoclusters (9 in total) using the BP86 functional<sup>24,25</sup> combined with the def2-SV(P)<sup>26</sup> basis set and the resolution of identities (RI) technique<sup>25,27,28</sup> as implemented in Turbomole 6.6. For the reaction mechanisms studied, all transition states and local minima were verified with frequency calculations. Key reaction paths were also calculated at the B3LYP<sup>29-31</sup> level of theory (hybrid density functional). Cohesive energy and free energy of formation calculations were performed to assess the stability of the nano-

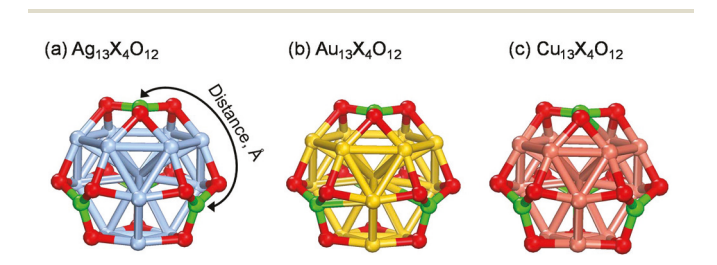


Fig. 1 Structural representation of (a)  $Ag_{13}X_4O_{12}$ , (b)  $Au_{13}X_4O_{12}$  and (c) Cu<sub>13</sub>X<sub>4</sub>O<sub>12</sub> nanoparticles where "X" (green atoms in the structures) for each chemical formula can be Al, Ga, or In. The approximate distance between each metal oxide center "X" is 5.4 Å, 5.0 Å, and 5.0 Å for Aq, Au, and Cu, respectively.

clusters. Eqn (1) was used to determine the cohesive energy (binding energy (BE) per atom (n)) of the nanoclusters:

$$\begin{aligned} \text{BE}/29 = & [E(\text{M}_{13}\text{X}_4\text{O}_{12}) - 13 \times E(\text{M}) - 4 \times E(\text{X}) \\ & - 12 \times E(\text{O})]/29 \end{aligned} \tag{1}$$

The cohesive energy quantifies the average bond strength, and thus, the stability, of the atoms forming the M<sub>13</sub>X<sub>4</sub>O<sub>12</sub> nanoclusters. The stability of the nanoclusters was also assessed with free energies of formation (egn (2)) calculated according to the following chemical reaction: 4Al(OH)3 +  $M_{13} \rightarrow M_{13}Al_4O_{12} + 6H_2$ :

$$\Delta G_{\rm f} = \left[ G({\rm M}_{13}{\rm X}_4{\rm O}_{12}) + 6 \times G({\rm H}_2) - G({\rm M}_{13}) - 4 \times G({\rm X(OH)}_3) \right] \tag{2}$$

where  $G(M_{13}X_4O_{12})$ ,  $G(H_2)$ ,  $G(M_{13})$ , and  $G(X(OH)_3)$  are the free energies of an isolated M13X4O12 nanocluster, an M13 nanocluster, a H<sub>2</sub> molecule, and a X(OH)<sub>3</sub> molecule, respectively.

#### Results and discussion

The stability of the  $M_{13}X_4O_{12}$  nanoclusters is shown in Fig. 2 and quantified in terms of cohesive energy (CE) as a function of M<sub>13</sub>X<sub>4</sub>O<sub>12</sub> nanocluster composition. The Cu<sub>13</sub>Al<sub>4</sub>O<sub>12</sub> nanocluster was determined as the most stable nanocluster with a CE of -101.52 kcal mol<sup>-1</sup> (negative values represent exothermicity). Furthermore, within each metal type we determined that the  $M_{13}X_4O_{12}$  nanoclusters containing aluminum (X = Al) were the most favorable structures. We have previously shown that the cohesive energy of M<sub>6</sub> (Ag, Au, Cu) clusters follows the trend (in kcal mol<sup>-1</sup>):  $|CE_{Cu} = -84.35| > |CE_{Au} = -34.68| >$  $|CE_{Ag} = -27.64|$ . The observed CE trend in this current work is reversed for Au and Ag in M<sub>13</sub>Al<sub>4</sub>O<sub>12</sub>: (|CE<sub>CuAl/Ga/In</sub>| >  $|CE_{AgAl/Ga/In}| > |CE_{AuAl/Ga/In}|$ ). However, just as with our pre-

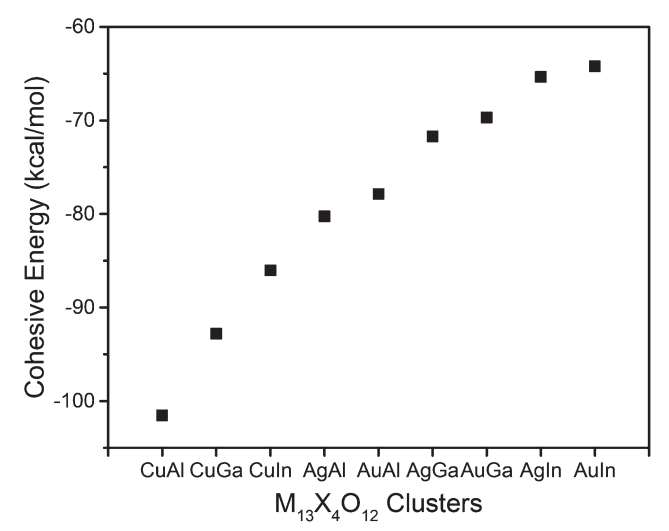


Fig. 2 Cohesive energy of the  $M_{13}X_4O_{12}$  clusters where M = Ag, Au, or Cu and X = Al, Ga, or In. The x-axis is abbreviated showing the MX combinations.

**Paper** 

vious work, the difference in CE values between Ag and Au (~2 kcal mol<sup>-1</sup> difference) is not as significant as the difference between Ag/Au and Cu (~22 kcal mol<sup>-1</sup> difference). Due to the stability of M<sub>13</sub>Al<sub>4</sub>O<sub>12</sub>, we selected these clusters for the analysis of the alcohol dehydration reactions to ether and olefin products. Specifically, we investigated the dehydration of ethanol to form ethylene via the concerted (E2) and sequential (Intramolecular - Intra.) mechanisms, and formation of DEE via the (competing)  $S_N$ 2 substitution reactions.

Fig. 3 illustrates the reaction energy profiles for E2 and intramolecular (Intra.) mechanisms on the M<sub>13</sub>Al<sub>4</sub>O<sub>12</sub> clusters for ethanol dehydration to ethylene. In recent publications the E2 mechanism has been shown to be preferred for alcohol dehydration over the sequential intramolecular pathway on Lewis acid sites, with the C-BH bond cleavage being rate-limiting in both mechanisms. Identically, we also found the sequential mechanism to exhibit significantly higher activation barriers (state V in Fig. 3) for the abstraction of a hydrogen atom from the β-carbon. As a result, we will focus on the E2 reaction mechanism as dominant on M13Al4O12 clusters for the remainder of this work.

The E2 activation energy barriers calculated on clusters in this work for ethanol dehydration to ethylene are comparable  $(E_a = \sim 31 \text{ kcal mol}^{-1})$  to those previously reported for pure alumina systems, performed at the B3LYP<sup>6,8,15</sup> ( $E_a = 32-37$ kcal  $\text{mol}^{-1}$ ) and PW91<sup>9</sup> levels of theory ( $E_a = 37 \text{ kcal mol}^{-1}$ ). The calculated alcohol dehydration activation barriers for the sequential (Intra.) and concerted (E2) mechanisms followed

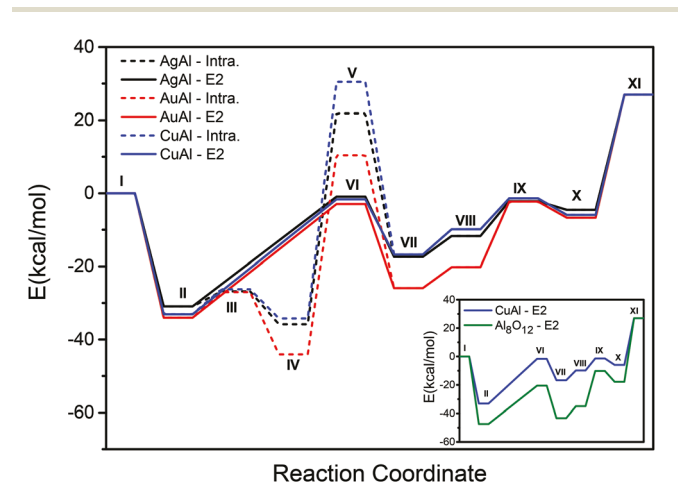


Fig. 3 Reaction pathways for ethanol dehydration on Ag<sub>13</sub>Al<sub>4</sub>O<sub>12</sub>, Au<sub>13</sub>Al<sub>4</sub>O<sub>12</sub>, Cu<sub>13</sub>Al<sub>4</sub>O<sub>12</sub> via the sequential (Intra.) and concerted (E2) reaction mechanisms. The roman numerals on each step represent: I. reference state with gas-phase molecular nanoclusters and ethanol in infinite separation, II. ethanol adsorption, III. TS1 in Intra. Mechanism with O-H bond dissociation, IV. ethoxide formation, V. TS2 in Intra. mechanism of ethylene formation, VI. TS for E2 concerted mechanism of ethylene formation, VII. physisorbed ethylene and chemisorbed dissociated water on the nanocluster, VIII. ethylene desorption, IX. TS for water formation, X. adsorbed water, and XI. final state with water desorption and the regeneration of the catalyst. The inset graph (bottom right) compares the reaction pathway for ethanol dehydration on the  $Cu_{13}Al_4O_{12}$  nanocluster to that of the pure alumina systems.

the trend Au < Ag < Cu and Ag < Au ≈ Cu in terms of core composition, respectively. The rate-limiting reaction barriers in the sequential pathway were calculated to be 57.66, 54.51, and 64.72 kcal mol<sup>-1</sup>, while those in the E2 pathway were calculated to be 29.98, 31.08, and 31.43 kcal mol<sup>-1</sup>, on Ag-, Au-, and Cu-based nanoclusters, respectively. In the inset graph located at the bottom right of Fig. 3 (solid green line: Al<sub>8</sub>O<sub>12</sub> and solid blue line: Cu<sub>13</sub>Al<sub>4</sub>O<sub>12</sub>), we compare the ethanol dehydration pathway on the Cu<sub>13</sub>Al<sub>4</sub>O<sub>12</sub> nanocluster (the most stable nanocluster from our CE calculations) to the pure alumina cluster (Al<sub>8</sub>O<sub>12</sub>, see ref. 8 and 15), with both systems exhibiting strong Lewis (tricoordinated) Al sites and treated at the BP86 level of theory. As shown in the inset of Fig. 3, the E2 activation energies of the pure alumina system (26.88 kcal mol<sup>-1</sup>) is lower than that on the Cu<sub>13</sub>Al<sub>4</sub>O<sub>12</sub> nanocluster. Although the pure alumina systems bind alcohol (-47.37 kcal mol<sup>-1</sup>) and water (-44.79 kcal mol<sup>-1</sup>) stronger, which contributes to the decrease of the dehydration barrier as a result of the recently identified structure-activity relationships in Lewis-acid-catalyzed alcohol dehydration reactions, 6,15 this strong binding leads to eventual deactivation of the catalyst by water poisoning17,18 (Sabatier principle). Due to the weaker interactions between the Cu<sub>13</sub>Al<sub>4</sub>O<sub>12</sub> nanocluster and ethanol (-33.08 kcal mol<sup>-1</sup>) and water (-32.91 kcal mol<sup>-1</sup>), less energy would be required to regenerate the bare Cu<sub>13</sub>Al<sub>4</sub>O<sub>12</sub> nanocluster, compared to the pure alumina analogue, making it a more active and robust alcohol dehydration catalyst. Fig. 4 shows the optimized geometries of elementary steps involved in the reaction mechanism for alcohol dehydration to ethylene on the Cu<sub>13</sub>Al<sub>4</sub>O<sub>12</sub> nanocluster. To further address the reaction energy profiles for ethylene formation on the Cu<sub>13</sub>Al<sub>4</sub>O<sub>12</sub> nanocluster compared to the pure alumina system, we repeated the calculations using the hybrid B3LYP functional. We found that the results generated using the B3LYP functional agreed very well with the observations at the BP86 level (Fig. S1†).

The olefin and the ether formation pathways are shown to be competing during ethanol dehydration. 10,13 DEE formation has been shown to occur via the S<sub>N</sub>2 mechanism, requiring coadsorption of two alcohols on neighboring Lewis acid sites (see example of Al sites on γ-Al<sub>2</sub>O<sub>3</sub> positioned at a distance of  $\sim$ 3.7 Å). However, the distance between the Al centers on the nanoclusters in this study varies between 5.0 and 5.4 Å (as shown in Fig. 1) due to the significant curvature of the metal core. Consequently, the interaction of two ethanol molecules chemisorbed on Al sites to form DEE is not feasible. An alternative etherification route involves the chemisorption of one alcohol reacting with an additional physisorbed alcohol (Fig. 5). The two interacting alcohols (one chemisorbed and one physisorbed as shown in structure II of Fig. 6) react through a concerted transition state (III in Fig. 6) in which DEE and a dissociated, surface-bound OH-H form in a single step (IV in Fig. 6). Subsequent desorption of DEE and water complete the catalytic cycle. The detailed reaction energy profile for DEE formation is shown in Fig. 5. Compared to the unimolecular (E2) pathway for olefin (i.e. ethylene) formation, olefin formation is energetically preferred ( $E_{\text{olefin}}^{\text{a}} = 31.43$ 

Nanoscale

Fig. 4 Graphical representations of elementary reaction steps reported in Fig. 3 for the competing ethylene formation mechanisms, using the  $Cu_{13}Al_4O_{12}$  nanocluster as an example. The roman numerals above each structure correspond to individual energetic states of reaction steps reported in Fig. 3.

kcal mol $^{-1}$  vs.  $E^{a}_{ether}=51.08$  kcal mol $^{-1}$ ), highlighting the structure-based selectivity of these nanocatalysts. Since the etherification barrier on  $\text{Cu}_{13}\text{Al}_4\text{O}_{12}$  was shown to be prohibitively high, the barriers were not calculated for the remaining nanoclusters. The E2 pathway for olefin formation on the same catalyst is also plotted in Fig. 5 for comparison. In the ESI $^{\dagger}$  we report the alcohol dehydration reaction energy paths for ethylene (E2) and DEE ( $\text{S}_{\text{N}}$ 2) formation on the  $\text{Cu}_{13}\text{Al}_4\text{O}_{12}$  nanocluster, calculated using the B3LYP functional. We found that the results generated at the B3LYP level were in agreement with the BP86 calculations (Fig. S2 $^{\dagger}$ ).

The use of these potentially highly selective nanoclusters in catalysis relies on their feasibility to be synthesized in the lab. Thus, to verify the synthesis potential of our novel nanocatalysts, we performed free energy of formation calculations at 500 K (represents the typical operating conditions in alcohol dehydration reactions) on the synthesis of the  $M_{13}Al_4O_{12}$  nanoclusters, using eqn (2).

We calculated the formation free energies of all three clusters and found that the energies followed the trend:  $\Delta G_{Cu}$  $(-148.1 \text{ kcal mol}^{-1}) < \Delta G_{Ag} (117.8 \text{ kcal mol}^{-1}) < \Delta G_{Au}$ (232.4 kcal mol<sup>-1</sup>). This formation energy trend follows what has been reported for CeO<sub>x</sub> particles supported by Au(111), Ag(111), and Cu(111).33 Our results showed that the most stable (most negative CE) catalyst in our study, the Cu<sub>13</sub>Al<sub>4</sub>O<sub>12</sub> system, was the most thermodynamically favored, while the formation of Au<sub>13</sub>Al<sub>4</sub>O<sub>12</sub> and Ag<sub>13</sub>Al<sub>4</sub>O<sub>12</sub> was thermodynamically uphill. The Cu<sub>13</sub>Al<sub>4</sub>O<sub>12</sub> system, in addition to being a very active and selective alcohol dehydration catalyst, has the potential of being synthesized according to our thermodynamic analysis. It should be noticed that these metal-oxide-protected metal nanoclusters resemble the thiolate-protected metal nanoclusters. For example, the experimentally synthesized Au<sub>25</sub>(SR)<sub>18</sub> nanocluster<sup>34</sup> consists of a 13-atom metal core, stabilized by a thiolate shell network, exhibiting 12 contacts with the core.35 Similarly, in our work the

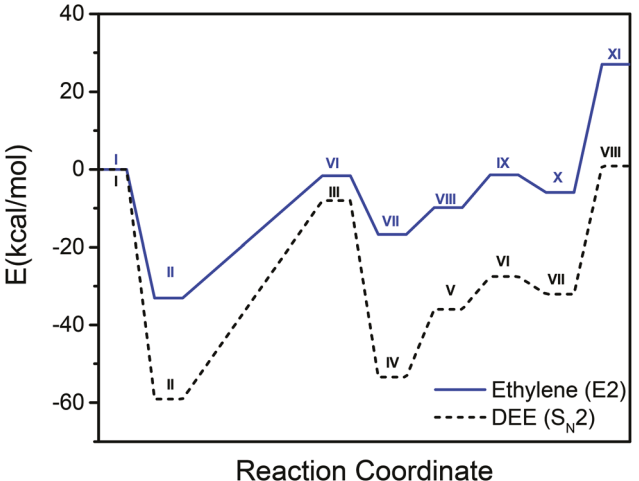


Fig. 5 Reaction pathway energetics for DEE and ethylene formation on  $\text{Cu}_{13}\text{Al}_4\text{O}_{12}$  via the  $\text{S}_{\text{N}}\text{2}$  (black dashed line) and E2 mechanism (blue line), respectively. The roman numerals on each step of the DEE mechanism represent: I. reference state with the gas phase nanocatalyst and the two ethanol molecules in infinite separation, II. both ethanol molecules coadsorbed on the nanocluster (one chemisorbed and the other physisorbed), III. DEE formation TS, IV. physisorbed DEE and chemisorbed dissociated water on the nanocluster, V. DEE desorption, VI. water formation TS, VII. formation of adsorbed water, and VII. water desorption and regeneration of the nanocluster. The description of the roman numerals for ethylene formation (in blue) are the same as presented in the caption of Fig. 3.

 $\rm M_{13}Al_4O_{12}$  nanoclusters consist of a 13-atom metal core, protected by an oxide shell that makes 12 contacts (O-bonds) with the core.

Overall, the nanoscale engineering of these novel  $M_{13}Al_4O_{12}$  nanocatalysts shown in this work is a unique example of *in silico* rational catalyst design, utilizing composition and morphology (size/shape) of metal and metal–oxide systems to design stable and highly selective alcohol dehydration catalysts. This is made feasible by shutting down non-preferred (bimolecular) reaction pathways through designing active sites on high-curvature nanoparticle surfaces. As a result, we report the first computational design of nanocatalysts that selectively convert ethanol to ethylene avoiding the DEE formation.

#### Conclusions

In this work, we use electronic structure calculations to design novel nanostructures, consisting of a metallic core and a metal-oxide shell of the form  $M_{13}X_4O_{12}$  (where M=Cu, Ag, and Au, and X=Al, Ga, and In), able to selectively dehydrate ethanol to ethylene. These nanocatalysts effectively catalyze the unimolecular (E2) dehydration of ethanol, while avoiding bimolecular reactions responsible for diethylether formation, due to the high curvature of the catalysts. We also determine that these nanoclusters can be more efficient dehydration catalysts than pure alumina systems by minimizing the energy required to regenerate the catalyst during reactions. In addition to designing these highly active and selective nanocatalysts our work demonstrates evidence of their potential synthesis; the nanoclusters were determined to be exothermically formed with  $Cu_{13}Al_4O_{12}$  displaying the most energetic preference.

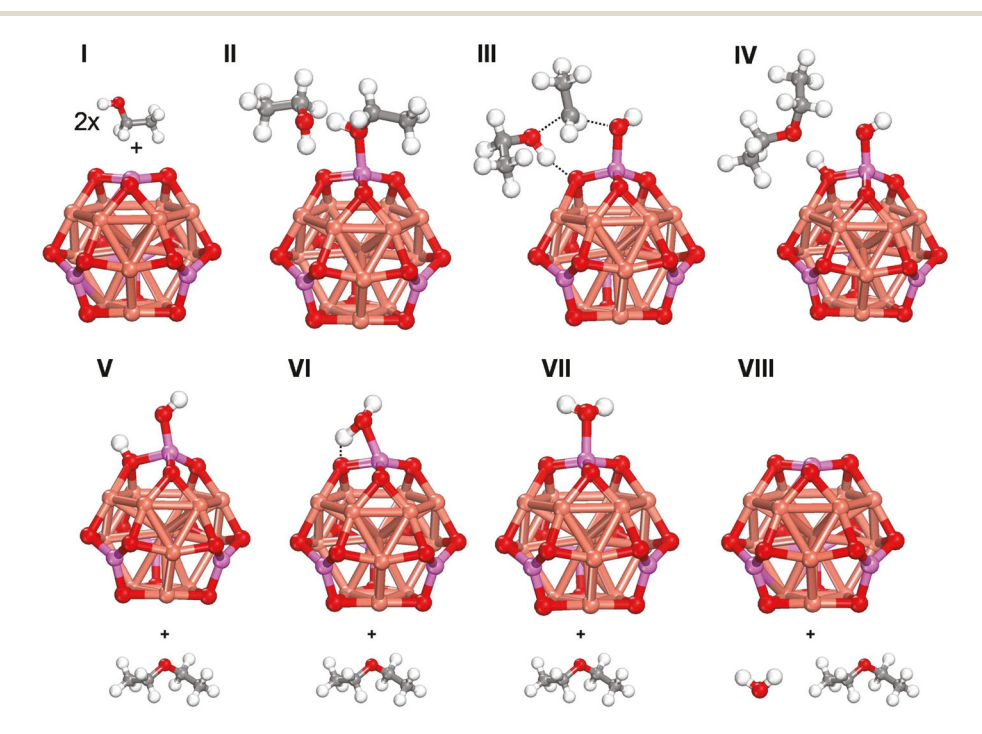


Fig. 6 Graphical representations of elementary reaction steps reported in Fig. 5 for the ether formation mechanism on the  $Cu_{13}Al_4O_{12}$  nanocluster. The roman numerals above each structure correspond to individual energetic states of reaction steps reported in Fig. 5.

Paper

To the best of our knowledge, this is the first demonstration of *in silico* rational catalyst design at the nanoscale for selective

#### Conflicts of interest

dehydration of alcohols to olefins.

Nanoscale

There are no conflicts to declare.

## Acknowledgements

This material is based upon work supported by the National Science Foundation (CBET-CAREER program) under Grant No. 1652694. N. A. would also like to acknowledge support from the National Science Foundation Graduate Research Fellowship Program under Grant No. (1247842). The authors would like to acknowledge the computational support from the University of Pittsburgh Center for Research Computing and the Extreme Science and Engineering Discovery Environment (XSEDE), which is supported by the NSF (ACI-1053575).

#### References

- 1 E. L. Kunkes, D. A. Simonetti, R. M. West, J. C. Serrano-Ruiz, C. A. Gartner and J. A. Dumesic, *Science*, 2008, 322, 417–421.
- 2 D. M. Alonso, J. Q. Bond and J. A. Dumesic, *Green Chem.*, 2010, 12, 1493–1513.
- 3 J. N. Chheda, G. W. Huber and J. A. Dumesic, *Angew. Chem., Int. Ed.*, 2007, **46**, 7164–7183.
- 4 M. Stocker, Angew. Chem., Int. Ed., 2008, 47, 9200-9211.
- 5 R. J. Gorte, Catal. Lett., 1999, 62, 1-13.
- 6 P. Kostestkyy, J. Yu, R. J. Gorte and G. Mpourmpakis, *Catal. Sci. Technol.*, 2014, 4, 3861–3869.
- 7 J. Macht, M. J. Janik, M. Neurock and E. Iglesia, *J. Am. Chem. Soc.*, 2008, **130**, 10369–10379.
- 8 S. Roy, G. Mpourmpakis, D.-Y. Hong, D. G. Vlachos, A. Bhan and R. J. Gorte, *ACS Catal.*, 2012, 2, 1846–1853.
- 9 M. A. Christiansen, G. Mpourmpakis and D. G. Vlachos, ACS Catal., 2013, 3, 1965–1975.
- 10 H. Knözinger and R. Köhne, J. Catal., 1964, 3, 559–560.
- 11 J. F. DeWilde, H. Chiang, D. A. Hickman, C. R. Ho and A. Bhan, *ACS Catal.*, 2013, 3, 798–807.
- 12 M. J. Kang, J. F. DeWilde and A. Bhan, *ACS Catal.*, 2015, 5, 602–612.

- 13 J. F. DeWilde, C. J. Czopinski and A. Bhan, *ACS Catal.*, 2014, 4, 4425–4433.
- 14 P. Kostestkyy, J. P. Maheswari and G. Mpourmpakis, *J. Phys. Chem. C*, 2015, **119**, 16139–16147.
- 15 P. Kostetskyy and G. Mpourmpakis, *Catal. Sci. Technol.*, 2015, 5, 4547–4555.
- 16 G. R. Jenness, M. A. Christiansen, S. Caratzoulas, D. G. Vlachos and R. J. Gorte, *J. Phys. Chem. C*, 2014, **118**, 12899–12907.
- 17 M. Digne, P. Sautet, P. Raybaud, P. Euzen and H. Toulhoat, J. Catal., 2002, 211, 1-5.
- 18 M. Digne, P. Sautet, P. Raybaud, P. Euzen and H. Toulhoat, J. Catal., 2004, 226, 54–68.
- 19 K. Larmier, C. Chizallet, N. Cadran, S. Maury, J. Abboud, A.-F. Lamic-Humblot, E. Marceau and H. Lauron-Pernot, ACS Catal., 2015, 5, 4423–4437.
- S. Eck, C. Castellarin-Cudia, S. Surnev, K. C. Prince,
   M. G. Ramsey and F. P. Netzer, *Surf. Sci.*, 2003, 536, 166–176.
- 21 J. A. Rodriguez and J. Hrbek, Surf. Sci., 2010, 604, 241-244.
- 22 J. A. Rodriguez, S. Ma, P. Liu, J. Hrbek, J. Evans and M. Perez, *Science*, 2007, 318, 1757–1760.
- 23 S. D. Senanayake, D. Stacchiola and J. A. Rodriguez, *Acc. Chem. Res.*, 2013, **46**, 1702–1711.
- 24 J. P. Perdew, Phys. Rev. B: Condens. Matter, 1986, 33, 8822– 8824.
- 25 K. Eichkorn, F. Weigend, O. Treutler and R. Ahlrichs, *Theor. Chem. Acc.*, 1997, 97, 119–124.
- 26 F. Weigend and R. Ahlrichs, *Phys. Chem. Chem. Phys.*, 2005, 7, 3297–3305.
- 27 K. Eichkorn, O. Treutler, H. Ohm, M. Haser and R. Ahlrichs, *Chem. Phys. Lett.*, 1995, **240**, 283–289.
- 28 F. Weigend, Phys. Chem. Chem. Phys., 2006, 8, 1057– 1065.
- 29 A. D. Becke, J. Chem. Phys., 1993, 98, 5648-5652.
- 30 C. T. Lee, W. T. Yang and R. G. Parr, *Phys. Rev. B: Condens. Matter*, 1988, 37, 785–789.
- 31 P. J. Stephens, F. J. Devlin, C. F. Chabalowski and M. J. Frisch, J. Phys. Chem., 1994, 98, 11623–11627.
- 32 N. Austin and G. Mpourmpakis, *J. Phys. Chem. C*, 2014, **118**, 18521–18528.
- 33 J. Graciani, A. B. Vidal, J. A. Rodriguez and J. F. Sanz, *J. Phys. Chem. C*, 2014, **118**, 26931–26938.
- 34 M. Zhu, E. Lanni, N. Garg, M. E. Bier and R. Jin, *J. Am. Chem. Soc.*, 2008, **130**, 1138–1139.
- 35 M. G. Taylor and G. Mpourmpakis, *Nat. Commun.*, 2017, 8, 15988.